

Article

Integrated Information on the Structure and Composition of the Ostrich Eggshell (*Struthio camelus*)

Alberto Pérez-Huerta ^{1,*}, Jean-Philip Brugal ², Murielle Salomé ³, Clemens N. Z. Schmitt ⁴
and Yannicke Dauphin ^{4,5,*}

¹ Department of Geological Sciences, The University of Alabama, Tuscaloosa, AL 35487, USA

² Aix Marseille Université, CNRS, Minist. Cult., UMR 7269 LAMPEA, 13097 Aix-en-Provence CEDEX 2, France

³ ID 21, European Synchrotron Radiation Facility, 71 Avenue des Martyrs, CS 40220, 38043 Grenoble CEDEX 9, France

⁴ Department of Biomaterials, Max Planck Institute of Colloids and Interfaces, 14424 Potsdam, Germany

⁵ ISYEB, UMR 7205, CNRS Muséum National d'Histoire Naturelle, Sorbonne-Université, EPHE, 75005 Paris, France

* Correspondence: aphuerta@ua.edu (A.P.-H.); yannicke.dauphin@sorbonne-universite.fr (Y.D.)

Abstract: Ostrich eggshells are excellent examples of avian biomineralization. Interest in these eggshells is focused on their potential as a food source, example of a biomaterial for medical and industrial applications, and the use of fossil remains for paleoenvironmental reconstructions. Due to this interest, there is some information about aspects of eggshell biomineralization, but it is scattered in different publications and is limited in scope about mineralogy-crystallography and/or composition. Here, we re-examine the biomineralization of the *Struthio* eggshells focusing on the structure, from macro- to nano-scales, crystallography, and composition of mineral and organic phases. Our results show that there is a very tight biomineralization control, from well-defined structures at nanoscale to precise crystallographic orientation of calcite crystals, in the formation of a biomineral that is unparalleled in other avian eggshells. Overall, this finding would explain the thickness and excellent mechanical properties of ostrich eggshells.

Keywords: organics; calcite; crystallography; nanoscale; biomineralization



Citation: Pérez-Huerta, A.; Brugal, J.-P.; Salomé, M.; Schmitt, C.N.Z.; Dauphin, Y. Integrated Information on the Structure and Composition of the Ostrich Eggshell (*Struthio camelus*). *Minerals* **2023**, *13*, 481. <https://doi.org/10.3390/min13040481>

Academic Editor: Olev Vinn

Received: 18 February 2023

Revised: 26 March 2023

Accepted: 27 March 2023

Published: 29 March 2023



Copyright: © 2023 by the authors. Licensee MDPI, Basel, Switzerland. This article is an open access article distributed under the terms and conditions of the Creative Commons Attribution (CC BY) license (<https://creativecommons.org/licenses/by/4.0/>).

1. Introduction

Mineralized eggshells, temporary structures in the life of birds and some reptiles, are natural biocomposites or bioceramics, composed of calcium carbonate and organics, that provide more or less efficient mechanical and microbial protection to the embryos. These shells are porous to control the inner humidity and oxygenation inside the egg, and they also represent an elemental reservoir for the mineralization of the bones of the embryo. Among eggshells, those produced by chickens are used as study models for eggshell biomineralization because they are sufficiently big for manipulation and are produced in about 22 h. Beyond the role of eggs as food resources, the shell is a source of inspiration to create new biomaterials. The inner organic membranes are used as template for crystal growth, to improve osteogenic activity, whereas mineral microparticles are used to reinforce synthetic materials [1–3]. Additionally, they are used to manufacture hydroxyapatite, which, in its form as powdered apatite, is used for surgical purposes [4–6].

Nys et al. [7] noted that “the general structure of the eggshell is basically the same in all avian birds” but, as for all biogenic minerals, numerous characteristics are species-dependent [8]. Avian eggshells are composed of several layers made of organic compounds and a mineral phase (low-Mg calcite), with the common descriptive nomenclature illustrated in Figure 1.

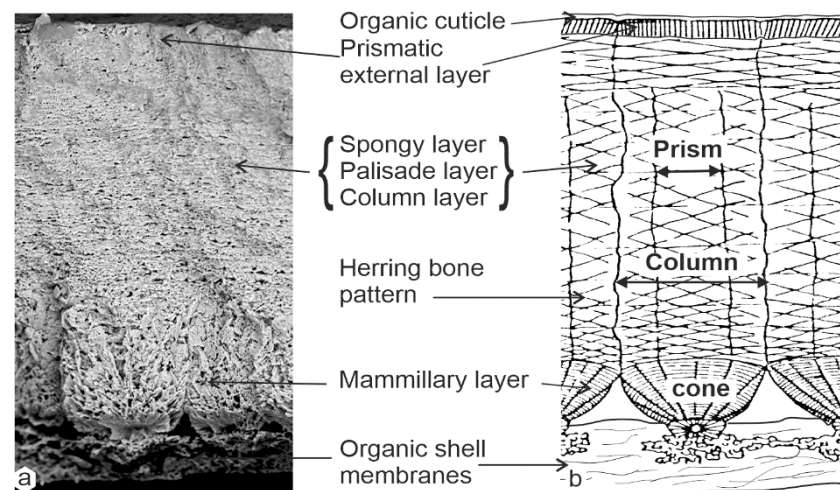


Figure 1. Descriptive structural terms of avian eggshells. (a) Scanning Electron Microscope picture of a broken avian eggshell across the shell thickness. (b) Schematic drawing and descriptive nomenclature used for avian eggshells (redrawn from Erben [8]).

Most of the structural and chemical data of eggshells is from very few taxa, mainly Neognathae and *Gallus gallus* as the main references. Erben [8], using scanning electron microscopy data, compared the structure of Palaeognathae (mainly flightless birds, ostrich included) and Neognathae (which includes chicken) eggshells. They share some features: the inner organic membranes, the mammillary layer with the granular center and the spherulitic structure, and the thick spongy or palisade layer with the herring bone pattern (Figure 1). Simple or complex pores are visible in cross section and, on the outer surface, a thin organic layer (cuticle) covers the surface. The intra-crystalline organic matrix of eggshells is composed of proteins, phosphoproteins, and sulphated acidic polysaccharides [9–16].

Giant eggshells assigned to Struthioniformes are known from Africa [17] and Asia [18,19] and, in general, ostrich eggshells are valued as food resources and ostrich farms are present in Europe, North America, Asia, and Australia. Additionally, ostrich eggshells are abundant in archaeological sites and used for paleoenvironmental [20] and social network reconstructions [21,22], and for phylogenetic purposes [23]. Nathusius [24] described the main layers of the ostrich eggshells (Figure S1a), including the radiating structure of the inner layer (Figure S1b) and the branching pores with complex openings (Figure S1c,d). The inner surfaces of these eggshells also show the difference between the mammillae with the organic layer (Figure S1e), and without this membrane (Figure S1f). Proteins are able to survive some diagenetic alterations in African samples [25]. The presence of an organic cuticle on the outer surface of the *Struthio* eggshell is still discussed [26–28]. The preservation of this thin organic layer probably depends on the environmental conditions of the nest and the freshness of the eggshell. In *Struthio camelus*, lipids are present [29], and some proteins have been identified [30,31].

In this study, we re-examine the structure (at micro- and nano-levels), composition, and crystallography of the eggshells of the ostrich *Struthio camelus*. The goal is to provide an integrated framework for a better understanding of the interplay between organic and mineral components of these eggshells. This information improves our knowledge on avian eggshell biomineralization and aids in the development of novel materials for industrial and medical applications.

2. Materials and Methods

2.1. Materials

Eggshells: *Struthio* eggshells come from wild animals and were collected in Namibia and Kenya, with some of them representing hatched and broken eggshells. Some fragments

were collected in nests; as a nest contains several eggs, it is difficult to ascertain the number of eggs we studied. Considering one specimen per egg, seven eggs is a plausible number. *Struthio camelus* is a Neornithes, Palaeognathae, Ratitae. Ostriches, not able to fly, are the largest modern birds and they are native to Africa. Ostriches lay an average of 45–50 eggs per year, and eggs are about 15 cm in length. Despite the large size of the eggs, the ratio between the size of the animal and that of the egg is one of the smallest among birds. The outer surface of the eggshell is white or yellowish white, and numerous pores are visible with the naked eye, whereas the inner surface is smooth. The average thickness of *Struthio camelus* eggshells is 2 mm [32], although it can reach 3.5 mm in fossil species.

Organic and Mineral Standards: Two organic standards have been used as references for FTIR analyses: type I collagen and chondroitin sulphate A. Collagen and chondroitin sulphate exist in the inner organic membranes [2,33,34]. Chondroitin sulphate, lipids and proteins were described in the spongy layer [35]. A calcitic speleothem was used as a reference for CaCO₃. Organic and mineral phosphorous-containing components have been used as standards for XANES analyses, and elemental phosphorous. Organic standards are glucose 6-phosphate, casein (for phosphoproteins), and phytic acid. Mineral standards are amorphous calcium phosphate (ACP), dicalcium phosphate (2Ca phosphate), tricalcium phosphate (3Ca phosphate), and geological apatite.

2.2. CT Scan-X-ray Computed Tomography

CT scan-X-ray computed tomography analyses were performed at the Natural History Museum, London. Data on the structure and pores of eggshells are obtained using the Metris X-Tek (Nikon Metrology) HMX ST 225 micro-CT system (Nikon, Tokyo, Japan) with a 4M pixel Perkin-Elmer detector (Perkin Elmer, Waltham, MA, USA) (voxel size 7.8 μm). X-rays were produced by focusing a 190 kV, 225 μA electron beam onto a molybdenum target. A collection of a series of 2D X-ray projection images by rotating the sample in the X-ray beam (cone-beam) by 0.1 degree increments over 360 degrees. The 2D X-ray projection images are reconstructed into a stack of serial 2D slices using the cone-beam back projection algorithms in Nikon Metrology CT Pro software. Rendering of the 3D structure of the sample is completed by assembling the separate 2D slices into a single 3D volume using FEI AVIZO9.3.0 software (FEI, Hillsboro, OR, USA). This software allows adjustment of the original rotation axis of the sample and acquisition of X-ray sections at any selected orientation.

2.3. Scanning Electron Microscope (SEM)

Eggshells were broken, fragments rinsed under tap water, and air dried at room temperature. Some fragments were observed without additional preparation, while others were embedded in resin, polished using diamond pastes down to a final 0.25 mm grade. Polished samples were cleaned with a detergent mixed with hot water for 1 min to remove any oil and diamond paste residues and rinsed with tap water and air dried at room temperature. Plasma etching was carried out with a Cemex system housed at the Swedish Museum of Natural History. Samples were in an atmosphere of oxygen and tetrafluoromethane (1/1 v/v) for 6h 30min at 35 W, so that the temperature increased is low and the samples are not damaged. The detailed procedures of the sample preparations are given in the figure legends. Au-Pd or C coated samples observations were conducted using a Philips 505, a Philips XL30 and a tabletop JCM 6000 SEM (Philips, Amsterdam, The Netherlands) in secondary electron mode (SE). Uncoated samples were examined using a FEI QUANTA FEG 600 (Max Planck Institute of colloids and interfaces, Potsdam, Germany) in a low vacuum, and secondary and back scattered electron (BSE) modes.

2.4. Atomic Force Microscopy

Samples were studied using a Nanoscope IIIa multi-mode scanning probe microscope operating in tapping mode (Max Planck Institute of colloids and interfaces, Potsdam, Germany). The tapping mode AFM utilizes an oscillating tip at amplitude of approximately

several tens of nm when the tip is not in contact with the surface. The resolution of tapping mode AFM is in the order of a few nm. Phase imaging is a powerful extension that goes beyond simple topographical mapping to detect variations in chemical composition, friction, and other physical properties. Compared with conventional secondary electron imaging SEM, AFM provides topographic direct height measurements and views of surface features since no coating is necessary. Moreover, three-dimensional AFM images are obtained without the difficult sample preparation (decalcification, thinning, etc.) of hard, mineralized samples necessary for high-resolution microscopy techniques.

2.5. Fourier Transform Infrared Spectroscopy (FTIR)

Eggshell fragments were dipped in sodium hypochlorite (NaClO) at a commercial concentration (2.6%) for 1 h to remove organic contaminants, then rinsed with Milli-Q H₂O and air dried. Cleaned fragments and KBr were reduced to a powder by grinding with an electric mortar for 10 min to obtain homogeneous granulometry. They were oven-dried at 38 °C overnight. Powdered samples and KBr were mixed (about 5% powdered samples in KBr) and loaded into the sample cup. All spectra were recorded at 4 cm⁻¹ resolution with 16 scans on a Perkin-Elmer Frontier Fourier transform infrared spectrometer (FTIR), in the wavenumber range 4000 to 450 cm⁻¹. The spectrometer was equipped with a Diffuse Reflectance accessory that permits DRIFT measurements with high sensitivity on powders. All spectra were corrected by the Kubelka–Munk function. The background spectrum was measured for pure KBr. Sample spectra were automatically ratioed against background to minimize CO₂ and H₂O bands. Correlation coefficients between two spectra of the same samples were about 99%.

2.6. Raman Spectroscopy

Pieces of untreated eggshells were embedded in Poly(methyl methacrylate) (PMMA) and polished to expose cross sections over the whole shell thickness. Raman spectra and images were obtained with a confocal Raman microscope (alpha300R, WITec, Germany) located at Max Planck institute of Colloids and Interface, Potsdam, Germany, and equipped with a 785 nm laser, which was focused on samples through a 20X objective (0.5 NA). The laser power on the sample was set to 10 mW for eggshells and 30 mW for the geological calcite standard. The spectra were acquired using a thermoelectrically cooled back-illuminated CCD detector behind a 600 g mm⁻¹ grating spectrograph (UHTS 300, WITec) with an average spectral resolution of 1 cm⁻¹ over a range of 2010 cm⁻¹. The software Control FIVE (Version 5.3, WITec) was used for measurement setup. Analysis of spectral data was performed with the software Project FIVE Plus (Version 5.2, WITec). Image scans were obtained over the full cross section of the eggshell. Since the laser power could not be adjusted to avoid burning of the inner membrane region, while allowing good quality measurements of the rest of the cross section, scan data was cut to only include data from unburned (i.e., not inner membrane) areas. Spectra of cut image scans with the same vertical position (i.e., lines of the image) were averaged (51 spectra for every line). The peak positions of these averaged spectra were measured by fitting a Gaussian function. The peak positions were then plotted as a function of their position along the eggshell cross-section thickness.

2.7. Electron Backscatter Diffraction (EBSD)

Fragments of eggshells were embedded in epoxy resin to observe cross sections throughout the shell thickness. Samples were grinded and subsequently polished with alumina of 1 µm and 0.3 µm. Polished samples were coated with a thin layer (2.5 nm) of carbon [36] and surrounded by silver paint to avoid electron charging. The EBSD study was carried out with an Oxford Nordlys camera attached to a field-emission JEOL 7000 FEG-SEM housed in the Alabama Analytical Research Center (AARC). Data were collected with the AZtec 2.0 software (Oxford Instruments, Oxford, UK) at high vacuum, 30 kV, large beam intensity, and a resolution of 1 µm step size or less for crystallographic maps.

Finally, data were analyzed using OIM 5.3 from EDAX-TSL. In this study, EBSD data are represented by diffraction intensity maps, crystallographic maps and pole figures, which represent the stereographic projection of crystallographic planes in reference to the {0001} calcite plane [37].

2.8. Electron Microprobe Analyses

Samples were embedded in resin and polished with diamond paste. Ultrasonic bath in water is not enough to remove the residual sticking contaminants (resin, diamond paste, etc.), so polished surfaces were slightly etched in 5% formic acid for 15 s to reveal structural details within the samples (e.g., different layers). The positions for analysis were chosen to reflect known structural features in the cross section of the eggshell. Measurements were made on carbon-coated samples.

Energy-dispersive X-ray microanalysis was undertaken with a Philips SEM505 SEM equipped with a solid-state X-ray detector. Quantitative analyses of elements were performed using the Link AN10000 analysis system with the ZAF/PB program that estimates peak-to-background element ratios. The ZAF/PB method can be applied to specimens with “rough surfaces”, essential for etched surfaces. Measurements were made using a lifetime of 100 s, an accelerating voltage of 15 kV, and a spot size of 100 nm or 200 nm. A cobalt standard provided the instrument calibration.

Maps and additional quantitative data were obtained on a Cameca SX50 (CAMECA, Gennevilliers, France) wavelength-dispersive electron microprobe at the Natural History Museum of London. For quantitative analysis, operating conditions used were 15 kV accelerating voltage and 20 nA specimen current. A minimum of 10 analyses were completed for each sample and the results averaged to obtain an individual sample mean. Elements analyzed were Ca, Fe, Mg, Na, P, S, and Sr.

2.9. Micro-XANES Spectroscopy Analyses (X-ray Absorption near Edge Structure)

The work was carried out at the ID21 X-ray micro-spectroscopy beamline of the European Synchrotron Radiation Facility (ESRF, Grenoble, France) using the Scanning X-ray Microscope. The beam was focused by a fixed-curvature Kirkpatrick–Baez mirrors system down to a submicron X-ray probe. The micro-probe was $0.3 \times 0.6 \mu\text{m}^2$ (vertical \times horizontal size) with 10^{10} photons/s. An energy dispersive Silicon Drift Diode (Bruker, Germany), with a collimated active area of 80 mm^2 and equipped with a thin polymer window, was used to collect the X-ray fluorescence (XRF) photons. An energy range between 2 keV and 7 keV is available at ID21, which gives access to the K-edge of phosphorus at 2.145 keV. The XANES energy scan at the P K-edge was achieved using a fixed-exit double-crystal Si(111) monochromator (Kohzu, Japan) located upstream the microscope. XANES spectra were acquired between 2.13 keV and 2.2 keV with 0.2 eV steps. The X-ray microscope was operated under vacuum to avoid the strong absorption of the phosphorus emission lines by air.

Although the primary beam energy was set around that of the P K-edge energy region, elements with absorption edges at lower energies were also subject to excitation and emission of fluorescence photons. Thus, micro-fluorescence element maps of Sr, Mg, and Na were obtained simultaneously with the P maps. Elemental peaks deconvolution was performed using the data analysis tool PyMCA [38].

The XANES spectra of all phosphorus samples used as standards have white line peak energies between 2152.69 eV and 2152.89 eV (Figure S2). All phosphorus minerals measured in this study contained phosphorus in the +V oxidation state. All white line peaks were found within the above energy range, but differences between mineral and organic samples were found. For in situ mapping and point analyses, eggshells were cut in cross sections throughout the shell thickness and embedded in epoxy resin. They were polished, then glued to a specific support for XANES analysis. Chemical compounds used as standards originates from Sigma-Aldrich (Munich, Germany) except for ACP. The ACP spectrum data used for performing the fit analyses was provided by Kim et al. [39] obtained

on the ID21 beamline. XANES spectra were normalized and analyzed with the ATHENA program of the IFFEFIT software package [40].

2.10. Extraction of the Organic Matrices

Eggshell fragments were soaked in NaClO at a commercial concentration for 1 h to remove organic contaminants of the eggshell surface and pores. Cleaned eggshells were rinsed with Milli-Q H₂O, then dried and ground into powder. They were decalcified in acetic acid at pH 5.5. The entire extract was centrifuged at 21,000× *g* for 15 min and separated into supernatant (soluble = SOM) and precipitated (insoluble = IOM) fractions. The insoluble fraction was desalted by successive centrifugations in Milli-Q H₂O and lyophilized. The soluble fraction was desalted by exchange with Milli-Q water on a Microconcentrator (Filtron) using a 3 kDa cut-off membrane and lyophilized.

3. Results

3.1. Structures

Aspect of the outer surface depends on the erosion of the eggshells; eggs are laid on the soil, often sandy, and they are regularly moved during the incubation to maintain a regular temperature. The most striking feature of the eggshell is the presence of pores on the outer surface, visible with naked eye (Figure 2a). These pores have multiple openings with diverse patterns (Figure 2b–d). Between pores, the polygonal pattern corresponds to the inner prismatic structures and some cracks (Figure 2e).

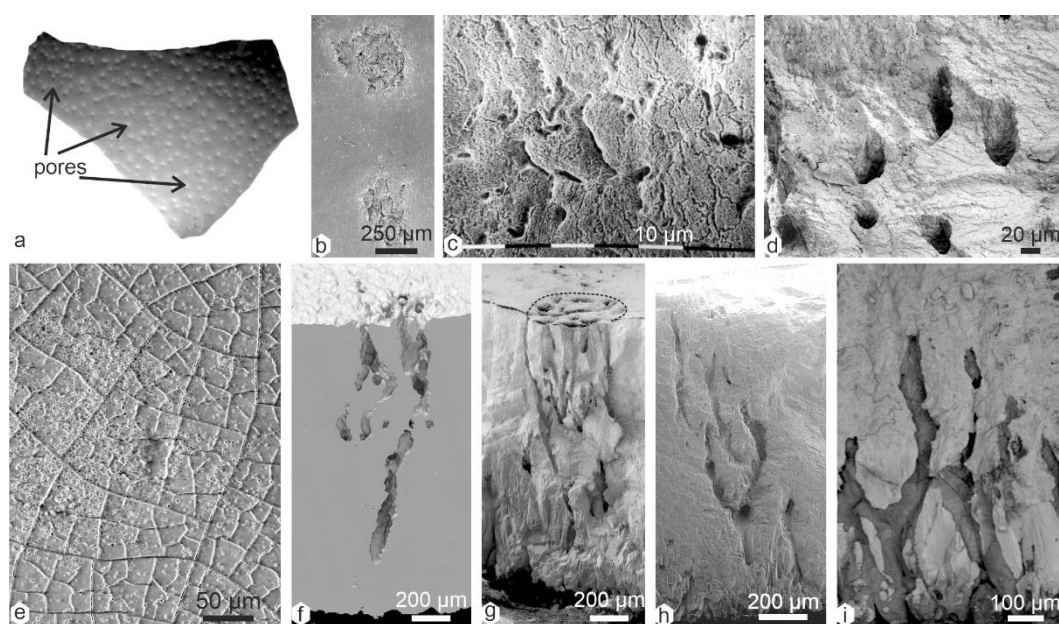


Figure 2. Pores of the eggshell. (a) Outer surface of a fragment showing the distribution of the pores. (b) SEM image of the outer surface showing two pores, the shape and size of which are different. (c,d) SEM images showing the multiple openings of pores and their irregular aspect. (e) Between the pores, the surface shows a polygonal pattern. (f) CT-scan reconstruction showing divergent canals from the inner side to the outer surface of the eggshell. (g) SEM views of the pore across the thickness of the eggshell; unetched fracture, (h,i) SEM BSE images showing the presence of an organic film (dark grey) lining the canals.

CT-scan reconstructions and SEM images of vertical fractures show the irregular and complex branched pores running from the inner to the outer surface of the eggshell (Figure 2f–i). The inner surface of the pores is grey, whereas between the pores, the layer is clearer in BSE SEM images (Figure 2i); an organic film seems to cover the inner surface of the pore and, at such magnification, the structure between the pores is not clearly visible.

Polished and lightly decalcified vertical sections show a similar structure at low magnification than to that originally described by Nathusius [24] (Figure S1a). Faint growth lines parallel to the outer surface of the eggshell are visible in the spongy layer, the main layer of the eggshell (Figure 3a). The spherulitic arrangement of the mammillary layer and pores is visible (Figure 3b). When the spherulitic units are broken, their tabular structure is distinct (Figure 3c). Depending on the orientation of the section, numerous small holes are visible (Figure 3d). The boundary between the mammillary layer and the spongy layer is not abrupt (Figure 3e), and the herring bone pattern is already well-built (Figure 3f). Prisms are more or less visible in the outer part of the prismatic layer (Figure 3a,g).

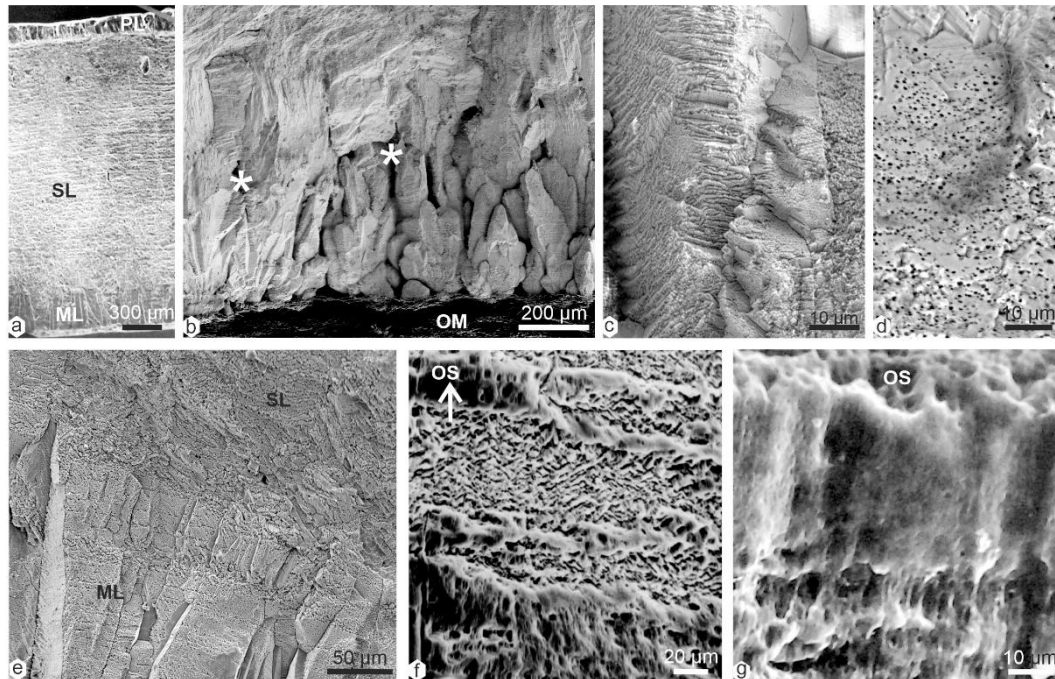


Figure 3. Microstructure of *Struthio* eggshell (vertical sections). (a) Vertical polished section showing the main mineralized layers, and faint growth lines in the spongy layer; compare to Figure S1a. Etched using H_3PO_4 10% for 30 s (b) Detail of the mammillary layer showing the divergent units, pores (*) and the inner organic layer (OM). (c) Inner structure of a prism showing calcitic tablets. Fracture cleaned using 0.001% acetic acid for 25 s Organic components removed using enzymatic solutions (alcalase, trypsin, and pronase in TRIS pH 7.5). (d) Vesicular holes in the divergent units of a spherulite cleaned with 0.001% acetic acid for 25 s (e) Same sample showing the transition between the mammillary layer (ML) and the spongy layer (SL); growth lines are visible in the mammillary layer; fracture cleaned using 0.001% acetic acid for 25 s Organic components removed using enzymatic solutions (alcalase, trypsin, and pronase in TRIS pH 7.5). (f) Polished and etched section (H_3PO_4 10% for 30 s) showing the first layers of the spongy layer and the herring bone pattern. (g) Same sample showing the thin outer prismatic layer. Abbreviations: ML: mammillary layer, SL: spongy layer, PL: outer prismatic layer, OS: outer surface, OM: organic layer.

Reconstructed inner surface shows regular protuberances (Figure 4a). SEM images show that protuberances are mineralized mammillae when the organic membranes are more or less removed (Figure 4b). The innermost surface of the inner layer of these organic membranes shows a dense radial network of organic fibers (Figure 4c). When the membranes are not present, the spherulitic structure of the calcified mammillae is revealed (Figure 4d). The organic network of fibers of the outer organic membrane is not dense (Figure 4e), and individual nodular fibers are visible (Figure 4f). Larger magnification of the surface of these fibers does not display an inner structure, except for some nodules (Figure 4g). Nevertheless, numerous small holes and some striations are visible on fibers

submitted to a plasma etching (Figure 4h, arrows), showing that these fibers are heterogeneous. When the inner organic membranes are destroyed, mineral units of the basal part of the spherulites appear to be angular (Figure 4i).

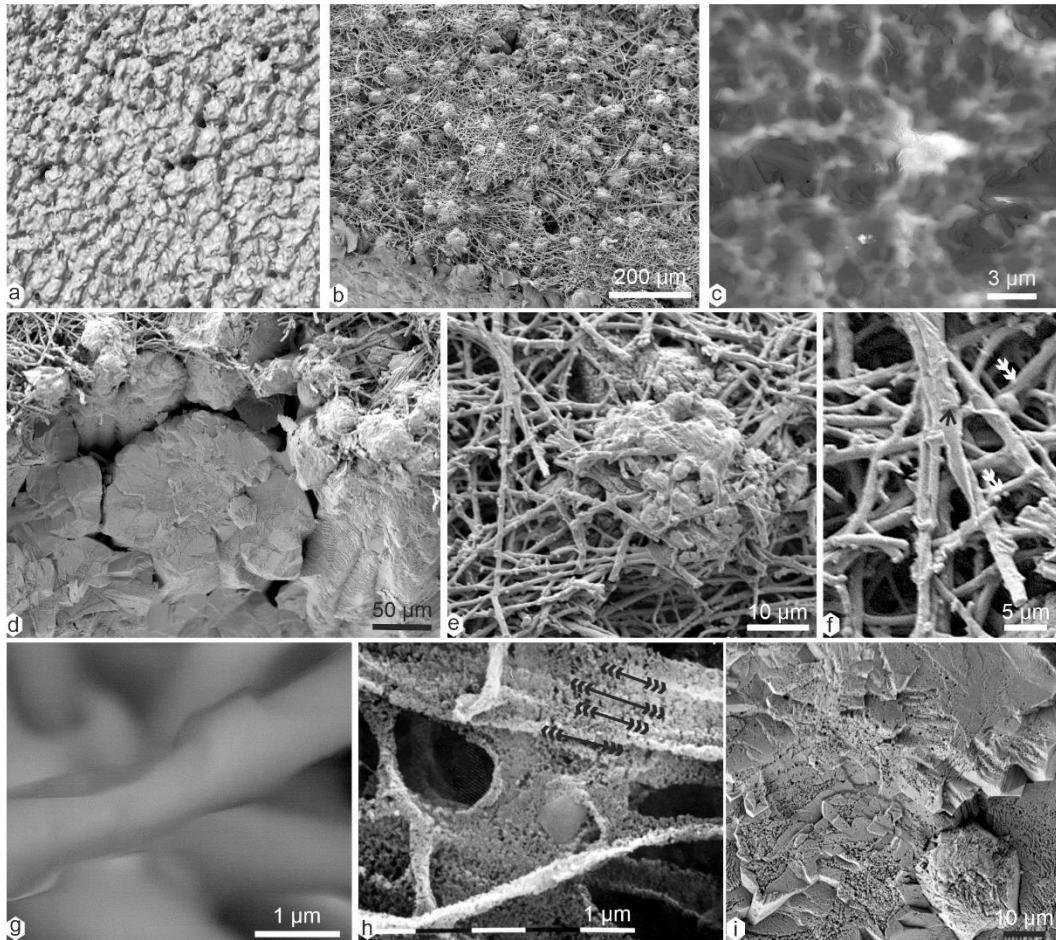


Figure 4. Structures of the inner surface of *Struthio* eggshell. (a) CT-scan reconstruction of the inner surface showing numerous protuberances. (b) More or less dissolved central part of the mammillae; H_3PO_4 10% for 10 s (c) Inner surface showing the mineralized mammillae and remains of the inner organic membranes. (d,e) Detail of the topographic relationships between the organic fibers and the first mineralized structures of the mammillary layer; inner organic membrane partially destroyed. (f) Elongated fibers with nodules (double arrows) and a bi-layered section (black arrow); unetched sample. (g) Detail of the same, showing a smooth surface; SEM image. (h) Plasma etching of the organic fibers shows they are heterogeneous; parallel striations are visible (arrows); oxygen/freon 1/1 35 W for 6h 30. (i) Aspect of the mammillary layer when the organic membrane is absent; etched with formic acid 10% for 1 min.

Additional features are visible at a nanoscale (Figure 5). The crystallites of the herring bone pattern of the spongy layer are flat rectangles, as shown by AFM phase contrast image (Figure 5a). It must be noted that in height image, i.e., topographic image (Figure 5b), the herring bone pattern visible in phase image contrast (Figure 5c) is not apparent. Phase contrast images of sections across the thickness of a rectangular tablets show that they are composed of aligned rounded granules (Figure 5d). The diameter of the granules is about 100 nm, and they are surrounded by a thin cortex (Figure 5e,f). Moreover, in phase contrast image (Figure 5e), the color of a single granule is not flat, suggesting its composition is not homogeneous. Similar granules are visible in the spherulites (Figure 5g), and in the central zone of the mammilla (Figure 5h), remains of the organic membranes show some elongated structures in phase contrast image (Figure 5i). Transverse zonations with irregular thickness

are visible, and very thin longitudinal striations. Locally, a fold suggests that this structure is soft and organic (Figure 5i, arrow).

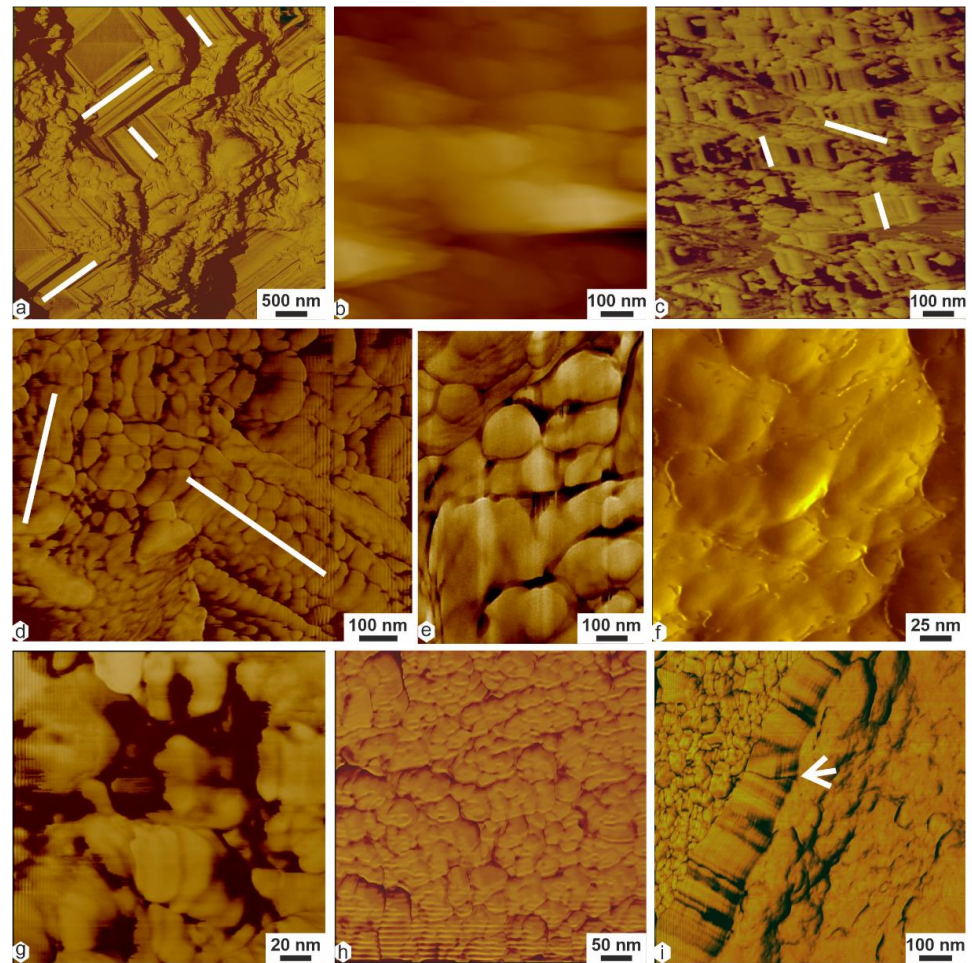


Figure 5. Nanostructure of *Struthio* eggshell. (a) Vertical section showing the herring bone pattern of the spongy layer; AFM phase contrast image. Polished and etched section (formic acid 10% for 10 s) (b) AFM height image does not show the herring bone pattern in a vertical section; acetic acid 10% for 20 s (c) Phase image contrast of the same zone showing the herring bone pattern. (d) More or less aligned rounded granules in the rectangular tablets; etched vertical section (formic acid 10% for 10 s) (e) Detail of the granules. Dark zones are more organic in phase image contrast. (f) Granules are surrounded by a thin cortex; AFM amplitude image, etched vertical section (formic acid 10% for 10 s) (g) Rounded granules in the spherulites. In black, remains of the inner organic membrane; phase image contrast, etched vertical section (acetic acid 10% for 10 s) (h) Inner surface of the mammillary layer. (i) Inner surface showing rounded granules and a banding pattern (arrow). The main part of the dry inner organic membrane was spontaneously detached. AFM phase image contrast.

3.2. Bulk Composition–Mineralogy

A comparison of Diffuse Reflectance Infrared Fourier Transform spectra (DRIFT) data of the powdered eggshell (Figure 6a) and organic and mineral standards (Figure 6b) shows that the eggshell is an organo-mineral composite. Bands assigned to CO_3^{2-} are in the range of calcite: ν_1 at 1085 cm^{-1} , ν_2 doublet at $876\text{--}848\text{ cm}^{-1}$, and ν_4 at 713 cm^{-1} (Figure 6a). A weak band at 559 cm^{-1} is assigned to PO_4 , whereas amide bands (amide A at $\sim 3300\text{ cm}^{-1}$, amide II, and 1795 cm^{-1}) are absent in the pure non-biogenic calcite, and those at 2982 cm^{-1} and 2512 cm^{-1} , respectively. These bands are very weak in the non-pure sample that we used.

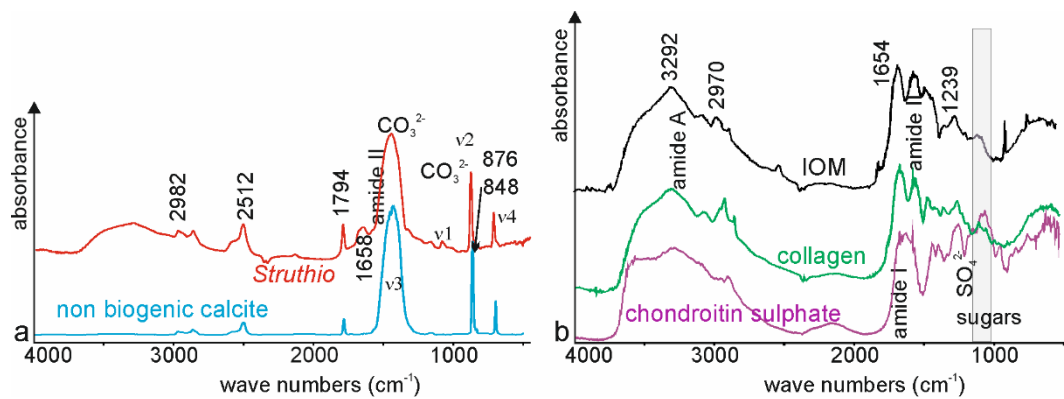


Figure 6. FTIR spectra of *Struthio* eggshell, organic, and mineral standards; powdered samples DRIFT method. (a) Spectrum of the powdered eggshell (*Struthio*) showing the main carbonate bands for calcite and bands for organic components, and a non-biological calcite. (b) Insoluble organic matrix (IOM) extracted from the eggshell and organic standards.

Organic standards used as references are collagen for protein and chondroitin sulphate for sugars (Figure 6b). Strong bands are at 3292 cm⁻¹ (amide A, β -sheet), and 2970 cm⁻¹ (C-H group, lipids, or O-H carboxylic acid). Several bands are present in the amide I region (1669, 1654, 1647, and 1636 cm⁻¹, respectively), indicative of complex structures. Four main bands are present in the amide II region (1560, 1540, 1522, and 1508 cm⁻¹). Strong amide I and II bands are also present in chondroitin sulphate. The sugar region (1150–1050 cm⁻¹) shows one weak band (1075 cm⁻¹) in the organic matrix; this region, absent in protein spectra, is usually considered to be characteristic of only sugars. The main part of the inner organic membranes has been removed, but the presence of organic remains attached to the mammillae cannot be excluded. The insoluble organic matrix (IOM) obtained after decalcification of the powdered eggshell shows amide I and amide II bands similar to those of collagen, and a bump in the SO₄²⁻ region (Figure 6b). Band at 1239 cm⁻¹ can be assigned to alanine, amide II, and/or glycosaminoglycans rich in S.

The characteristic Raman modes of calcite are the translational crystal lattice vibration at 156 cm⁻¹, rotational lattice vibration at 282 cm⁻¹, v₄ in-plane C-O bending at 712 cm⁻¹, and v₁ symmetric C-O stretching at 1086 cm⁻¹ [41]. These peaks are present in spectra of the outer, spongy, and inner areas of the eggshell cross section along the line indicated in the inset of Figure 7a. While the spectra of the eggshell are in good agreement with the calcite standard, there are substantial peak shifts to higher wavenumbers (up to 1.3 cm⁻¹) toward the inside and outside of the eggshell cross section. The shift of the 1086 cm⁻¹ peak is plotted as a function of the measurement position over the thickness of the mineral part of the eggshell cross-section in Figure 7b. It must be noticed that amorphous calcium carbonate is not detected in these mature and dry samples.

3.3. Crystallography

Electron backscatter diffraction (EBSD) analyses were conducted on surfaces across the eggshell thickness. These analyses confirm the calcitic composition of the eggshell and the presence of inter- and intra-crystalline organics represented by regions and/or pixels with no diffraction (dark areas) (Figures 8 and 9). The spongy layer (Figure 8a–c) is characterized by large calcite crystals with the *c*-axis parallel to the elongation of the crystals. In contrast, the mammillary layer (Figure 8d–f) shows a more random crystallographic orientation of the calcite due to small crystals alternating orientation with the calcite *c*-axis parallel (red/pink colors) and perpendicular (green/blue colors) to the base of the cones (Figure 8e,f). Additionally, these layers present more regions with no diffraction due to the abundance of organics. Lastly, the outer layer (Figure 9) contains well-defined, large calcite crystals with the *c*-axis perpendicular to the outer shell surface.

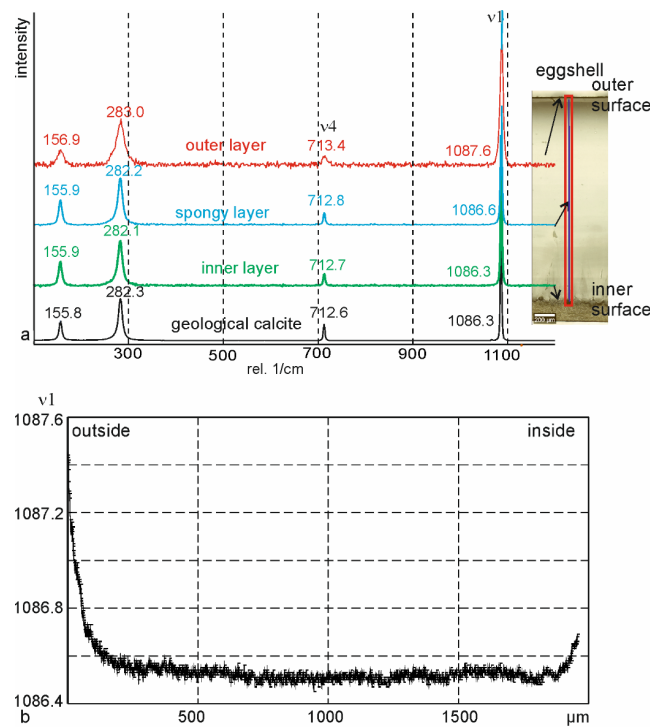


Figure 7. Raman data for the *Struthio* eggshell. (a) Raman spectra of different regions along the cross section of the eggshell and of non-biogenic calcite showing bands characteristics for calcite. The inset shows the correlating area of the eggshell cross-section for the spectra. The red box indicates the scan area. The blue line in the red box indicates the horizontal axis of the shift-plot in (b). (b) Shift of the v1 band as observed when moving from the outside to the inside of the eggshell cross-section.

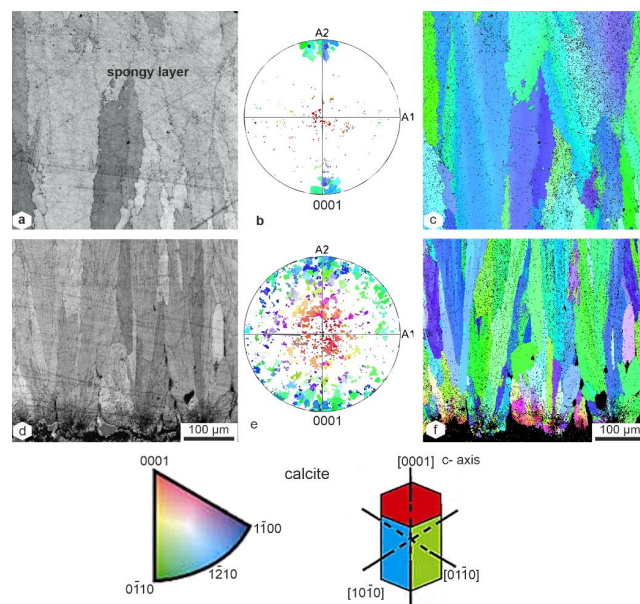


Figure 8. Electron backscatter diffraction (EBSD) for the *Struthio* eggshell. (a–c) Data from the spongy layer and (d–f) data for the mamillary layer: (a,d) represent diffraction intensity maps, with higher diffraction indicated by lighter colors and no diffraction by dark regions; (c,f) represent color-coded crystallographic maps, with the colors relating to crystallographic planes, as shown in the color-key legends at the bottom; and (b–e) represent the stereographic projections of the orientations of calcite crystals in the crystallographic map in relation to the {0001} plane of calcite. [Note: A1 and A2 in the stereographic projections are reference axes that relate to the position of the sample in relation to the electron beam and EBSD camera].

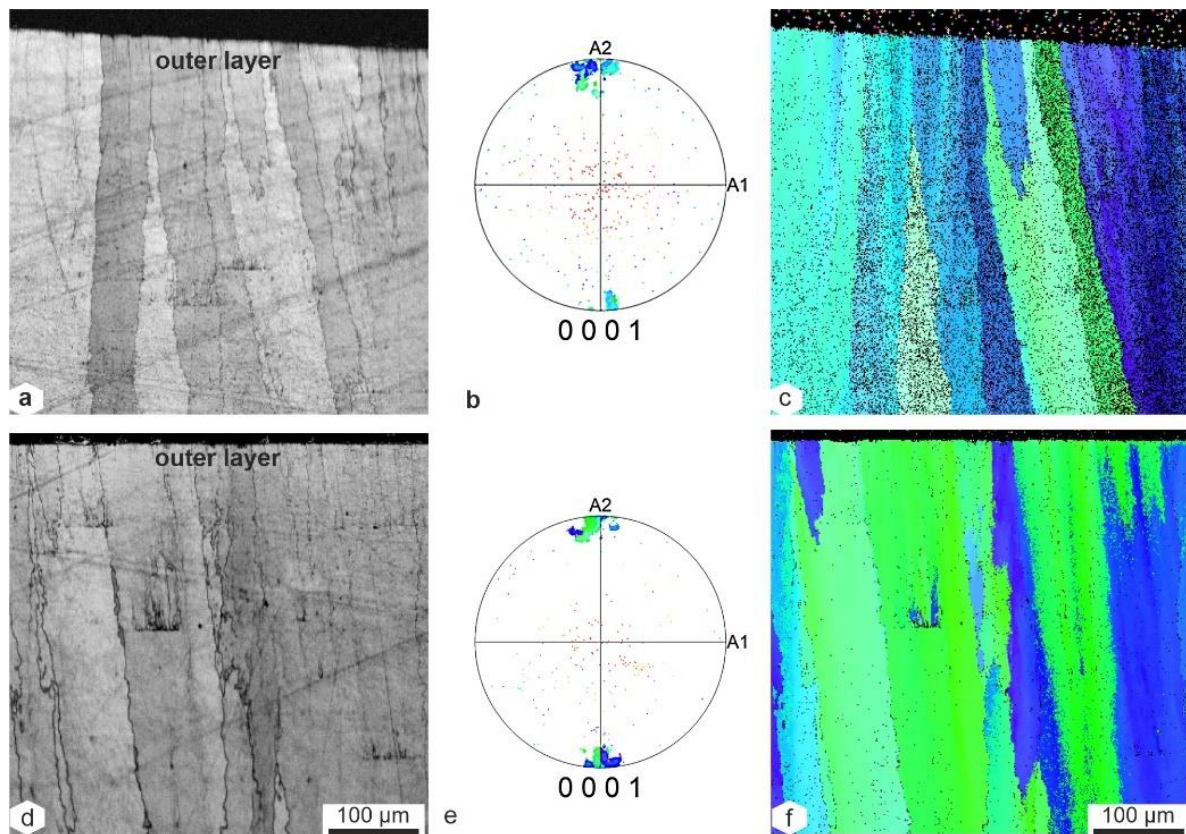


Figure 9. Electron backscatter diffraction (EBSD) for two regions within the outer layer of the *Struthio* eggshell. (a,d) represent diffraction intensity maps, with higher diffraction indicated by lighter colors and no diffraction by dark regions; (c,f) represent color-coded crystallographic maps with the colors relating to crystallographic planes, as shown in the color-key legends at the bottom of Figure 8; and (b–e) represent the stereographic projections of the orientations of calcite crystals in the crystallographic map in relation to the {0001} plane of calcite. [Note: A1 and A2 in the stereographic projections are reference axes that relate to the position of the sample in relation to the electron beam and EBSD camera].

3.4. Chemical Composition

Electron microprobe quantitative analyses show that the average Mg content of the eggshell is that of a low Mg calcite (Figure S3a). P, S, and Fe contents are low, but easily detected by the electron microprobe. However, the average content does not reveal the trends throughout the thickness of the shell (Figure S3b). The basal parts of the mammillae are rich in Mg and P (Figure S3b,f–g), while the outer prismatic layer also shows a slight increase in these elements (Figure S3b). Mg distribution map shows the concentric structure of the mammillae (Figure S3f); this structure is faintly visible in P map (Figure S3g). The sulfur map is flat, except for a small zone between the spherulites and rich in organic matrix (inner membranes; Figure S3h). The borders of the spherulites are rich in P.

Elemental distribution maps of Mg and Na for the whole section of the eggshell show that the inner mammillary zone and the outer layer are enriched in these elements in comparison to the main part of the mammillary and the columnar layers (Figure 10a–f). The borders between the mammillae are also well visible in detailed Mg and Na maps. The Sr distribution map is more homogenous (Figure 10g), but detailed maps show that the inner part of the mammillae has higher Sr content than the outer part (Figure 10h,i).

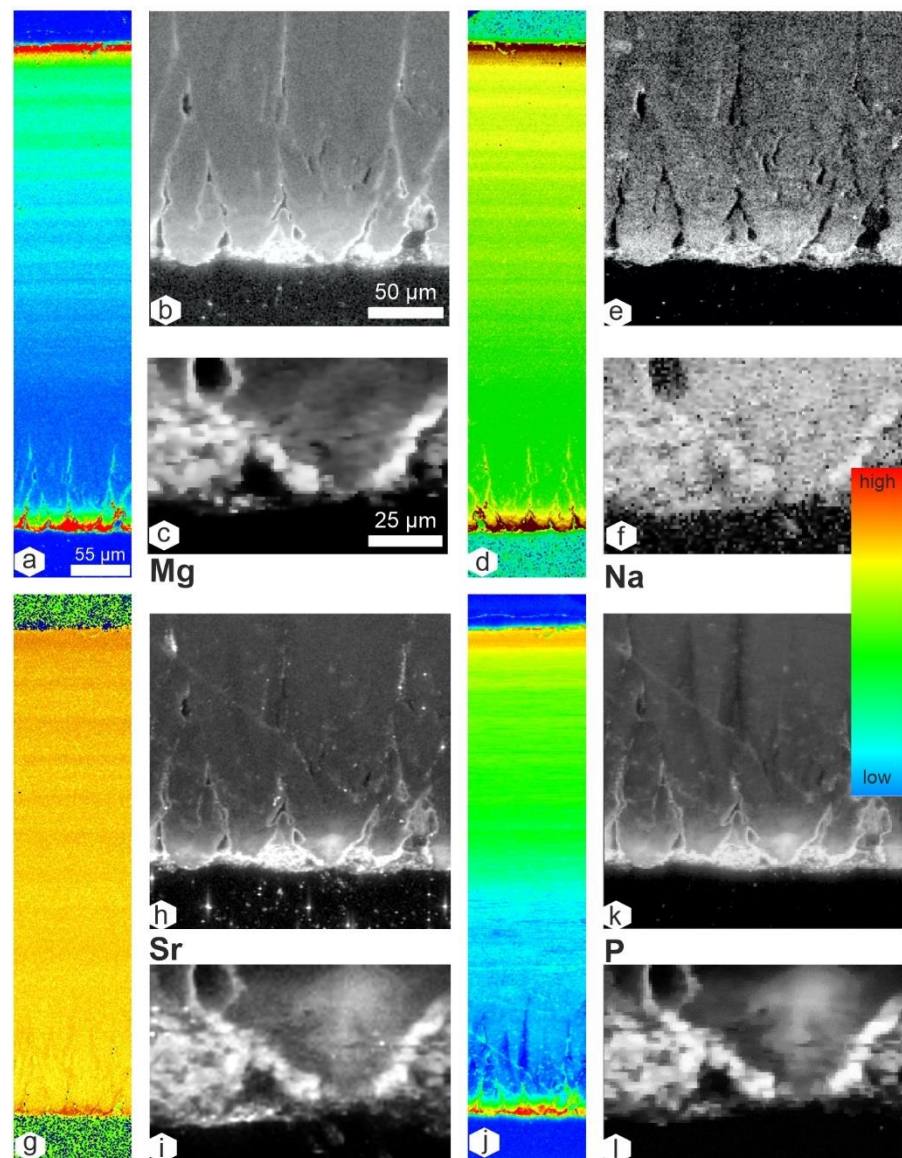


Figure 10. Chemical maps across the eggshell. Mg, Na, and Sr: elemental maps, P: XANES map at the P K edge. The mammillary layer and the outer prismatic layer are rich in Mg (a–c) and Na (d–f). Inner regions are richer in Mn and Na than the outer region; these trends are less visible in Sr map (g–i). XANES maps are similar to that of Mg (j–l).

All P samples exhibit a main peak around 2152 eV, but two features differentiate the mineral and organic P samples (Figure S2). Mineral P samples exhibit a small shoulder at approximately 2157 eV, whereas a regular peak is observed at this level for organic P samples. Moreover, the broad smooth peak centered around 2167 eV for the organic samples and ACP is subdivided in two broad peaks for the mineral samples [42,43]. This broad peak is absent in elemental P (Figure S2). The map at 2152 eV shows that the inner organic membranes are rich in P (Figure 10j, red zone). The P content of the mammillary layer and a part of the columnar layer is low, then increases toward the outer surface (Figure 10j).

In situ XANES spectra show similar profiles (Figure 11). The small but distinct peak at 2161 eV visible from the mammillary layer to the outer prismatic layer does not exist in minerals. The spectra of the extracted organic matrices are similar, but not identical: the soluble organic matrix has a smooth bump at 21,687 eV, meanwhile, the insoluble matrix has two small peaks within the bump (21,675 and 21,694 eV) (Figure 11).

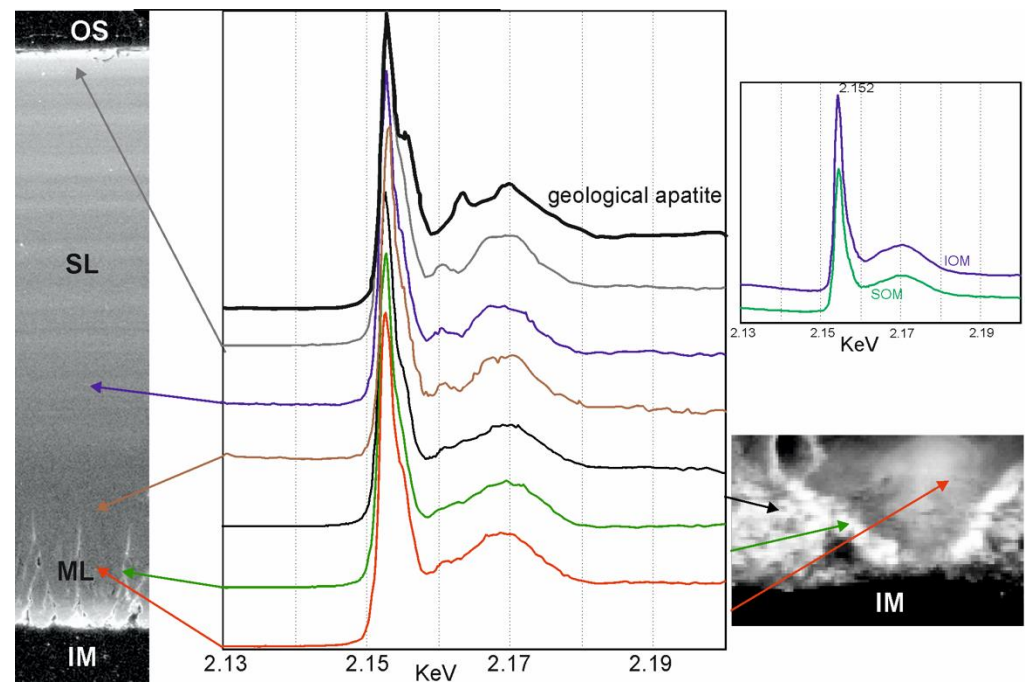


Figure 11. In situ P K edge spectra across the eggshell from extracted organic matrices (IOM and SOM) and a non-biogenic apatite showing that P is “organic” in the eggshells. OS: outer surface; SL: spongy layer; ML: mammillary layer; IM: inner organic membranes.

4. Discussion and Concluding Remarks

4.1. Structure

The presence of an outer organic membrane is still discussed for *Struthio* eggshells [26,44]. The confusion is maintained because the inner organic membrane—the white membrane between the mineralized eggshell and the white albumin soft part—is sometimes called the outer membrane [28]. In fact, wild ostriches lay and hatch eggs on the soil, so that the outer organic cuticle is usually eroded during the pre-incubation period. Then, eggs are moved during incubation, probably to maintain temperature. When eggs are broken, they are submitted to higher temperature, dry conditions, and the inner organic membranes are dissociated from the mammilla. Thus, the aspect and preservation of the inner and outer surfaces depend on environmental conditions and our data cannot add new information to the debate about organic membranes. However, the presence of an organic layer connected to the outer cuticle, and its connection to the pores, is not clear in previous studies. We observe the branching pattern of pores that is characteristic of *Struthio* shells, and our SEM-BSE images confirm the presence of an organic coating on the walls of the pores, which is also displayed in various taxa [45–47].

The herring bone pattern described by Erben [8] and Richards et al. [27], called crisscross pattern by Mikhailov [48], seems to be built by elongated acicular crystallites. According to Mikhailov [48], “the submicroscopic elements . . . are subrhombic plates . . . These plates . . . can be decomposed into minute plate subunits . . .”. In our SEM images, the “plates” are cubic. The crystallographic analysis of Chien et al. [49] have shown that the “acicular crystallites”, visible in polished sections of chicken eggshells, are rectangular thin platelets. This is in accordance with our AFM phase contrast images of oblique sections showing that this structure is made of stacked rectangular platelets, the orientation of which regularly changes. A closer examination shows that the rectangular platelets are themselves made of aligned rounded granules. Tabular structures in the spherulites were already described [8,48]. AFM results show that prisms, spongy layer, and spherulitic units are composed of rounded granules (diameter between 50 nm and 100 nm), surrounded by a thin cortex, as shown by amplitude and phase contrast mode images. According to Haugstad [50], and Mittal and Matsko [51], a soft material is usually “darker” than a

hard material. Thus, it can be suggested that the thin cortex is rich in organic components. Similar granules have been observed in the eggshell of *Numida*, *Anser*, and *Gallus* [47,52].

Diameter of the vesicular holes is smaller than 1 μm . This size is in agreement with those of Palaeognathae eggshells: between 0.3 μm to 1.2 μm [46]. The size of the vesicular holes does not seem related to the size or thickness of the eggshell [34].

The inner membrane is composed of two layers: an inner compact and dense one, the “outer” layer comprises a complex network. The fibrous structure of the inner organic membranes is described in the works of Nathusius [24], but few studies are dedicated to the structure of the fibers. Transmission electron and scanning electron microscope observations have shown that the fibers are layered structure and that their diameters vary within a single eggshell [53–55] with protuberances common along the fibers [46].

4.2. Mineralogy–Crystallography

FTIR and Raman spectra show that the eggshell is calcite. FTIR wavenumbers of the v4 band at 712.8 cm^{-1} are indicative of low Mg contents [56,57]. Ratio of the maximal intensity in normalized spectra of v2 vs. v4 bands is 1.47 and corresponds to a crystalline state [58]. As described by Rodriguez-Navarro et al. [59], the first mineralized deposit is ACC but, in the mature eggshell, only calcite is detected. FTIR bands of vaterite and calcite are similar (v2 doublet), but v4 at 745 cm^{-1} exists only in vaterite [60]. This band is absent in the studied samples. A precise interpretation of organic bands is difficult because there is significant overlap and hundreds of molecules (more than 697 proteins have been detected [61]). Raman analyses confirm that the main components is calcite, and the narrow peaks are indicative of a well crystallized form, with the potential exception of the inner surface (spherulitic structures of the mammillary layer) and in agreement with EBSD diffraction results. EBSD data also confirms the calcitic composition of these eggshells and, in general, EBSD results are in agreement with those reported by Dalbeck and Cusack [62], and Jain et al. [19] for fossil samples. The outer (prismatic) and spongy layers show high crystallinity and a strong preferred orientation of calcite crystals, whereas the mamillary layer presents two preferred crystallographic orientations of calcite related to differences in crystal sized and steps in the eggshell formation. These results are in agreement with previous data obtained with X-ray Diffraction (XRD) and EBSD [19,62–65]. Among avian eggshells, ostrich eggshells present the highest level of crystallographic control and, interestingly, are only comparable to that reported in some dinosaur eggshells [66].

4.3. Composition

In situ analyses show heterogeneous distribution of the main chemical elements throughout the thickness of the eggshell. Raman spectra show shifts of the C-O v1 and v4 bands in scans over the thickness of eggshell cross sections (Figure 7). These shifts correlate with the variation of Mg and P detected in the elemental maps (Figure 10 and Figure S3). This correlation has been shown previously to enable the determination of Mg content in calcite [64,65]. Based on these previous studies and the observed shifts of the v1 band, the Mg content in ostrich eggshells is low and varies between about 7 mol% and 13 mol% over the cross section (Figure S4). Organic components, such as pigments, found in the outer organic membrane in some avian species, are not detected in cross sections [66].

Variations in the elemental composition are also visible in P and S. It must be noted that depending on the presence or absence of the inner organic membranes, these profiles differ. A basic analysis shows that Mg and P have the highest correlation coefficients (Table 1) (FIJI colocalization software). It is worth to note that despite Mg that is usually present in calcite, the species (organic or mineral) of Mg is not yet known. The high contents of Mg and P are in the mammillary layers (Figure S3), where the structure is not compact and dense, but composed of granules at nanoscale. EBSD has shown that *c*-axis of calcite of the mammillary layer are very variable and that this layer is poorly crystalline (Figure 8). Thus, it may be suggested that ACC is still present in the inner layer of the eggshell.

Table 1. Correlation coefficients showing the high colocalizations of the studied chemical elements, based on EDS elemental distribution maps. Plugins of FIJI colocalization software were used. Note that, although there are differences in the resulting correlation coefficients, the trends are similar.

	Mg/Na	Mg/Sr	Mg/P	Sr/Na	Sr/P	Na/P
Person-R-values	0.82	0.81	0.95	0.8	0.82	0.78
Spearman	0.55	0.64	0.93	0.45	0.68	0.51
Manders M1	1	0.96	0.98	1	1	1
Manders M2	0.999	1	1	0.935	0.985	0.96
Kendall	0.4	0.48	0.79	0.33	0.51	0.37

The presence of organic fibers inserted in the mammillae of the inner part of the eggshells does not help to estimate the mineral-organic ratios. It is not possible to destroy all the organic fibers of the inner membranes without a partial dissolution of the microcrystals of the mammillae; thus, the values obtained by TGA are variable. Chemical analyses show that the high sulfur contents of the inner organic membranes are in agreement with the presence of dermatan sulphate [34]. Sulphated sugars were identified in chicken eggshells [9,12]. Phosphates are present in chicken eggshells [67,68], but Mg and P are considered to be of mineral origin. From in situ XANES spectra or those obtained on extracted organic matrices, P components are organic and/or ACP. As FTIR and Raman analyses do not detect ACP, it is suggested that the main part of P is organic. The role of Mg and phosphate in the precipitation of CaCO₃ has been shown in *Gallus* [14]. Osteopontin, a phosphoglycoprotein, also performs a role in the formation of eggshells [10,16,34,47,69–71].

Eggshells of a small number of bird species have been described, but all known samples are composed of similar structural layers, except for the inner organic membranes and outer pellicle. Despite an overall similarity, the structure, crystallinity, and composition of the eggshells are species-dependent, showing that the biomineralization process is strongly controlled by the organism. However, our integrated data shows that ostriches are unique among birds producing eggshells because such biological control is more pronounced. Eggshells are biomineral products generated relatively rapid (in less than 24 h), and thus, the structural and crystallographic control of the mineral-organic composite is not perfect, as previously shown for the eggshells of the guinea fowl and graylag goose [52]. However, ostrich eggshells present a strong hierarchical organization of structural units from the nano- to the macro-scale levels and a tight crystallographic control of calcite formation. This would explain the thickness of these eggshells and their superior mechanical properties, in particular to breakage [72], resulting in ideal models for bio-inspired materials and explaining the good preservation of fossil material.

Supplementary Materials: The following supporting information can be downloaded at: <https://www.mdpi.com/article/10.3390/min13040481/s1>, Figure S1: Nathusius drawings from [24]; Figure S2: XANES standards; Figure S3: Elemental composition; Figure S4: correlation between FTIR and electron microprobe analyses.

Author Contributions: Conceptualization, Y.D. and A.P.-H.; XANES analyses, M.S.; Raman analyses, C.N.Z.S.; A.P.-H.: EBSD analyses; Y.D.: SEM and AFM data; sample collections, J.-P.B.; writing, review and editing, Y.D. and A.P.-H. All authors have read and agreed to the published version of the manuscript.

Funding: This research was funded by ESRF grant number LS2371 and LS256.

Data Availability Statement: Not applicable.

Acknowledgments: Authors thank the three anonymous reviewers for their comments that have contributed to improve the manuscript. Additionally, authors thank the journal editorial team for assistance. Many thanks go to C.T. Williams and A. Denis for the support in chemical analysis with the electron microprobes. Finally, we are thankful to D. Werner (Max Planck institute for colloids and interfaces) for conducting CT-scan experiments.

Conflicts of Interest: The authors declare no conflict of interest.

References

1. Rovensky, J.; Stancikova, M.; Masaryk, P.; Svik, K.; Istok, R. Eggshell calcium in the prevention and treatment of osteoporosis. *Int. J. Clin. Pharmacol. Res.* **2003**, *23*, 83–92. [[PubMed](#)]
2. Arias, J.L.; Arias, J.I.; Fernandez, M.S. Avian eggshell as a template for biomimetic synthesis of new materials. In *Handbook of Biomineralization: Biological Aspects and Structure Formation*; Wiley: Hoboken, NJ, USA, 2007; pp. 109–118.
3. Chen, X.; Zhu, L.; Wen, W.; Lu, L.; Luo, B.; Zhou, C. Biomimetic mineralisation of eggshell membrane featuring natural nanofiber network structure for improving its osteogenic activity. *Colloids Surf. B Biointerfaces* **2019**, *179*, 299–308. [[CrossRef](#)] [[PubMed](#)]
4. Elizondo-Villarreal, N.; Martinez-de-la-Cruz, A.; Guerra, R.O.; Gomez-Ortega, J.L.; Torres-Martinez, L.M.; Casrano, V.M. Biomaterials from agricultural waste: Eggshell-based hydroxyapatite. *Water Air Soil Pollut.* **2012**, *223*, 3643–3646. [[CrossRef](#)]
5. Abdulrahman, I.; Tijani, H.I.; Mohammed, B.A.; Saidu, H.; Yusuf, H.; Jibrin, M.N.; Mohammed, S. From garbage to biomaterials: An overview on eggshell based hydroxyapatite. *J. Mater.* **2014**, *2014*, 802467. [[CrossRef](#)]
6. Macha, I.J.; Ozyegin, L.S.; Oktar, F.N.; Ben-Nissan, B. Conversion of ostrich eggshells (*Struthio camelus*) to calcium phosphates. *J. Austr. Ceramic. Soc.* **2015**, *51*, 125–133.
7. Nys, Y.; Gautron, J.; Garcia-Ruiz, M.; Hincke, M.E. Avian eggshell mineralization: Biochemical and functional characterization of matrix proteins. *Comptes Rendus Palevol.* **2004**, *3*, 549–562. [[CrossRef](#)]
8. Erben, H.K. Ultrastrukturen und mineralisation rezenter und fossiler eischalen bei vögeln und reptilien. *Biomineralization* **1970**, *1*, 1–66.
9. Picard, J.; Paul-Gardais, A.; Vedel, M. Glycoprotéines sulfates des membranes de l’oeuf de poule et de l’oviducte. *Biochim. Biophys. Acta* **1973**, *320*, 427–441. [[CrossRef](#)] [[PubMed](#)]
10. Pines, M.; Knopov, V.; Bar, A. Involvement of osteopontin in eggshell formation in the laying chicken. *Matrix Biol.* **1994**, *14*, 765–771. [[CrossRef](#)]
11. Hincke, M.T. Ovalbumin is a component of the chicken eggshell matrix. *Connect. Tissue Res.* **1995**, *31*, 227–233. [[CrossRef](#)]
12. Carrino, D.A.; Rodriguez, J.P.; Caplan, A.L. Dermatan sulfate proteoglycans from the mineralized matrix of the avian eggshell. *Connect. Tissue Res.* **1997**, *36*, 175–193. [[CrossRef](#)] [[PubMed](#)]
13. Mann, K. Isolation of a glycosylated form of the chicken eggshell protein ovocleidin and determination of the glycosylation site. Alternative glycosylation/phosphorylation at an N-glycosylation sequon. *FEBS Lett.* **1999**, *463*, 12–14. [[CrossRef](#)] [[PubMed](#)]
14. Hincke, M.T.; St Maurice, M. Phosphorylation-dependent modulation of calcium carbonate precipitation by chicken eggshell matrix proteins. In *Chemistry and Biology of Mineralized Tissues*; Goldberg, M., Boskey, A., Robinson, C., Eds.; American Academy of Orthopaedic Surgeons: Rosemont, IL, USA, 2000; pp. 13–17.
15. Gautron, J.; Hincke, M.T.; Panheleux, M.; Garcia-Ruiz, J.M.; Boldicke, T.; Nys, Y.Y. Ovotransferrin is a matrix protein of the hen eggshell membranes and basal calcified layer. *Connect. Tissue Res.* **2001**, *42*, 255–267. [[CrossRef](#)] [[PubMed](#)]
16. Hincke, M.T.; Chien, Y.C.; Gerstenfeld, L.C.; McKee, M.D. Colloidal-gold immunocytochemical localization of osteopontin in Avian eggshell gland and eggshell. *J. Histochem. Cytochem.* **2008**, *56*, 467–476. [[CrossRef](#)]
17. Pickford, M.; Mein, P.; Senut, B. Fossiliferous neogene karst fillings in Angola, Botswana and Namibia. *S. Afr. J. Sci.* **1994**, *90*, 227–230.
18. Sahni, A.; Kumar, G.; Bajpai, S.; Srinivasan, S. Ultrastructure and taxonomy of ostrich eggshells from Upper Palaeolithic sites of India. *J. Paleontol. Soc. India* **1989**, *34*, 91–98.
19. Jain, S.; Bajpai, S.; Kumar, G.; Pruthi, V. Microstructure, crystallography and diagenetic alteration in fossil ostrich eggshells from Upper Palaeolithic sites of Indian peninsular region. *Micron* **2016**, *84*, 72–78. [[CrossRef](#)]
20. Roberts, P.; Henshilwood, C.S.; van Niekerk, K.L.; Keene, P.; Gledhill, A.; Reynard, J.; Badenhorst, S.; Lee-Thorp, J. Climate, environment and early human innovation: Stable isotope and faunal proxy evidence from archaeological sites (98–59ka) in the Southern Cape, South Africa. *PLoS ONE* **2016**, *11*, e0157408. [[CrossRef](#)]
21. Miller, J.M.; Yiming, V.; Wang, Y.V. Ostrich eggshell beads reveal 50,000-year-old social network in Africa. *Nature* **2022**, *601*, 234–239. [[CrossRef](#)]
22. Diehl, R.J.; Keller, H.M.; Hodgkins, J. Towards an interpretive framework for heated ostrich eggshell: An actualistic study. *J. Archaeolog. Sci. Rep.* **2022**, *43*, 103465. [[CrossRef](#)]
23. Mikhailov, K.E.; Zelenkov, N. The late Cenozoic history of the ostriches (Aves: Struthionidae), as revealed by fossil eggshell and bone remains. *Earth-Sci. Rev.* **2020**, *208*, 103270. [[CrossRef](#)]
24. von Nathusius, W. Über die hüllen, welche den dotter des vogeles umgeben. *Z. Wissensch. Zool.* **1868**, *18*, 225–270.
25. Demarchi, B.; Hall, S.; Roncal-Herrero, T.; Freeman, C.L.; Woodley, J.; Crisp, M.K.; Collins, M.J. Protein sequences bound to mineral surfaces persist into deep time. *eLife* **2016**, *5*, e17092. [[CrossRef](#)]
26. Richards, P.D.G.; Richards, P.A.; Lee, M.E. Ultrastructural characteristics of ostrich eggshell: Outer shell membrane and the calcified layers. *J. S. Afr. Vet. Assoc.* **2000**, *71*, 97–102. [[CrossRef](#)] [[PubMed](#)]
27. Richards, P.D.G.; Botha, A.A.; Richards, P.A. Morphological and histochemical observations of the organic components of ostrich eggshell. *J. S. Afr. Vet. Assoc.* **2002**, *73*, 13–22. [[CrossRef](#)]
28. Szczerbinska, D.; Wiercinska, M. Ultrastructure of the eggshell of selected Palaeognathae species—a comparative analysis. *Ann. Anim. Sci.* **2014**, *14*, 167–178. [[CrossRef](#)]
29. Kriesten, K.; Egge, H.; Faust, R. Lipids in the eggshell of the ostrich (*Struthio camelus*). *Experientia* **1979**, *35*, 1032–1033. [[CrossRef](#)]

30. Mann, K.; Siedler, F. Ostrich (*Struthio camelus*) eggshell matrix contains two different C-type lectin-like proteins. Isolation, amino acid sequence, and posttranslational modifications. *Biochim. Biophys. Acta* **2004**, *1696*, 41–50. [[CrossRef](#)]
31. Reyes-Grajeda, J.P.; Marin-Garcia, L.; Stojanoff, V.; Moreno, A. Purification, crystallization and preliminary X-ray analysis of struthiocalcin 1 from ostrich (*Struthio camelus*) eggshell. *Acta Cryst.* **2007**, *F63*, 987–989. [[CrossRef](#)]
32. Tyler, C.; Simkiss, K. A study of the eggshells of ratite birds. *Zoology* **1959**, *133*, 201–243.
33. Arias, J.L.; Carrino, D.A.; Fernandez, M.S.; Rodriguez, J.P.; Dennis, J.E.; Caplan, A.I. Partial biochemical and immunochemical characterization of avian eggshell extracellular matrices. *Arch. Biochem. Biophys.* **1992**, *298*, 293–302. [[CrossRef](#)] [[PubMed](#)]
34. Hincke, M.T.; Nys, Y.; Gautron, J.; Mann, K.; Rodriguez-Navarro, A.B.; McKee, M. The eggshell: Structure, composition and mineralization. *Front. Biosci.* **2012**, *17*, 1266–1280. [[CrossRef](#)] [[PubMed](#)]
35. Simkiss, K.; Tyler, C. A histochemical study of the organic matrix of hen eggshells. *Quater. J. Micro. Sci.* **1987**, *98*, 19–28.
36. Perez-Huerta, A.; Cusack, M. Optimising electron backscatter diffraction (EBSD) of carbonate biominerals—Resin type and carbon thickness. *Microsc. Microanal.* **2009**, *15*, 197–203. [[CrossRef](#)]
37. Perez-Huerta, A.; Dauphin, Y.; Cuif, J.P.; Cusack, M. High resolution electron backscatter diffraction (EBSD) data from calcite biominerals in recent gastropod shells. *Micron* **2011**, *42*, 246–251. [[CrossRef](#)]
38. Solé, V.A.; Papillon, E.; Cotte, M.; Walter, P.; Susini, J. A multiplatform code for the analysis of energy-dispersive X-ray fluorescence spectra. *Spectrochim. Acta Part B* **2007**, *B62*, 63–68. [[CrossRef](#)]
39. Kim, B.; Gautier, M.; Rivard, C.; Sanglar, C.; Michel, P.; Gourdon, R. Effect of aging on phosphorus speciation in surface deposit of a vertical flow constructed wetland. *Environ. Sci. Technol.* **2015**, *49*, 4903–4910. [[CrossRef](#)]
40. Ravel, B.; Newville, M. Athena, Artemis, Hephaestus: Data analysis for X-ray absorption spectroscopy using IFEFFIT. *J. Synchr. Rad.* **2005**, *12*, 537–541. [[CrossRef](#)]
41. Stock, S.R.; Veis, A.; Xiao, X.; Almer, J.; Dorvee, J.R. Sea urchin tooth mineralization: Calcite present early in the aboral plumula. *J. Struct. Biol.* **2012**, *180*, 280–289. [[CrossRef](#)]
42. Brandes, J.A.; Ingall, E.; Paterson, D. Characterization of minerals and organic phosphorus species in marine sediments using soft X-ray fluorescence spectromicroscopy. *Mar. Chem.* **2007**, *103*, 250–265. [[CrossRef](#)]
43. Ingall, E.D.; Brandes, J.A.; Diaz, J.M.; de Jonge, M.D.; Paterson, D.; McNulty, I.; Elliott, W.C.; Northrup, P. Phosphorus K-edge XANES spectroscopy of mineral standards. *J. Synchr. Rad.* **2011**, *18*, 189–197. [[CrossRef](#)] [[PubMed](#)]
44. Willoughby, W.; Steyn, L.; Bam, L.; Oliver, A.J.; Devey, R.; Maina, J.N. Micro-focus X-Ray tomography study of the microstructure and morphometry of the eggshell of Ostriches (*Struthio Camerus*). *Anat. Rec.* **2016**, *299*, 1015–1026. [[CrossRef](#)]
45. Chien, Y.C.; Hincke, M.T.; Vali, H.; McKee, M.D. Ultrastructural matrix mineral relationships in avian eggshell, and effects of osteopontin on calcite growth in vitro. *J. Struct. Biol.* **2008**, *163*, 84–99. [[CrossRef](#)]
46. Becking, J.H. The ultrastructure of the avian eggshell. *Ibis* **1975**, *117*, 143–151. [[CrossRef](#)]
47. Athanasiadou, D.; Jiang, W.; Goldbaum, D.; Saleem, A.; Basu, K.; Pacella, M.S.; Böhm, C.F.; Chromik, R.E.; Hincke, M.T.; Rodríguez-Navarro, A.B.; et al. Nanostructure, osteopontin, and mechanical properties of calcitic avian eggshell. *Sci. Adv.* **2018**, *4*, eaar3219. [[CrossRef](#)]
48. Mikhailov, K.E. The principal structure of the avian eggshell: Data of SEM studies. *Acta Zool. Cracov.* **1987**, *30*, 53–70.
49. Chien, Y.C.; Hincke, M.T.; McKee, M.D. Avian Eggshell Structure and Osteopontin. *Cells Tissues Organs* **2009**, *189*, 38–43. [[CrossRef](#)]
50. Haugstad, G. *Atomic Force Microscopy: Understanding Basic Modes and Advanced Applications*; John Wiley and Sons: Hoboken, NJ, USA, 2012.
51. Mittal, V.; Matsko, N.B. *Analytical Imaging Techniques for Soft Matter Characterization*; Springer Science and Business Media: New York, NY, USA, 2012.
52. Pérez-Huerta, A.; Dauphin, Y. Comparison of the structure, crystallography and composition of eggshells of the guinea fowl and graylag goose. *Zoology* **2016**, *119*, 52–63. [[CrossRef](#)] [[PubMed](#)]
53. Masshoff, W.; Stolpmann, H.J. Licht-und Elektronenmikroskopische Untersuchungen and der Schalenaut und Kalschale des Hühnerieies. *Z. Zellforsch. Mikrosk. Anat.* **1961**, *55*, 818–832. [[CrossRef](#)]
54. Simons, P.C.M.; Wiertz, G. Notes on the structure of membranes and shell in the hen’egg—an electron microscopical study. *Z. Zellforsch.* **1963**, *59*, 555–557. [[CrossRef](#)]
55. Tan, C.K.; Chen, T.W.; Chan, H.L.; Ng, L.S. A scanning and transmission electron microscopic study of the membranes of chicken egg. *Histol. Histopath.* **1992**, *7*, 339–345.
56. Böttcher, M.E.; Gehlken, P.L.; Steele, D.F. Characterization of inorganic and biogenic magnesian calcites by Fourier transform infrared spectroscopy. *Solid State Ionics* **1997**, *101*, 1379–1385. [[CrossRef](#)]
57. Dauphin, Y. Infrared spectra and elemental composition in recent biogenic calcites: Relationships between the n4 band wavelength and Sr and Mg concentrations. *Appl. Spectrosc.* **1999**, *53*, 184–190. [[CrossRef](#)]
58. Beniash, E.; Aizenberg, J.; Addadi, L.; Weiner, S. Amorphous calcium carbonate transforms into calcite during sea urchin larval spicule growth. *Proc. R. Soc. Lond.* **1997**, *264*, 461–465. [[CrossRef](#)]
59. Rodríguez-Navarro, A.B.; Marie, P.; Nys, Y.; Hincke, M.T.; Gautron, J. Amorphous calcium carbonate controls avian eggshell mineralization: A new paradigm for understanding rapid eggshell calcification. *J. Struct. Biol.* **2015**, *190*, 291–303. [[CrossRef](#)]
60. Jones, G.C.; Jackson, B. *Infrared Transmission Spectra of Carbonate Minerals*; Chapman & Hall: London, UK, 1993; p. 233.

61. Mann, K.; Mann, M. The proteome of the calcified layer organic matrix of turkey (*Meleagris gallopavo*) eggshell. *Proteome Sci.* **2013**, *11*, 40. [[CrossRef](#)] [[PubMed](#)]
62. Dalbeck, P.; Cusack, M. Crystallography (Electron Backscatter Diffraction) and Chemistry (Electron Probe Microanalysis) of the Avian Eggshell. *Cryst. Growth Design.* **2006**, *6*, 2558–2562. [[CrossRef](#)]
63. Cain, C.J.; Heyn, A.N.J. X-ray Diffraction Studies of the Crystalline Structure of the Avian Egg Shell. *Biophys. J.* **1964**, *4*, 23–39. [[CrossRef](#)]
64. Silyn-Roberts, H.; Sharp, R.M. Crystal growth and the role of the organic network in eggshells. *Proc. R. Soc. Lond.* **1986**, *227*, 303–324.
65. Heredia, A.; Rodriguez-Hernandez, A.G.; Lozano, L.F.; Pena-Rico, M.A.; Velazquez, R.; Basiuk, V.A.; Bucio, L. Microstructure and thermal change of texture of calcite crystals in ostrich eggshell *Struthio camelus*. *Mater. Sci. Eng.* **2005**, *C25*, 1–9. [[CrossRef](#)]
66. Eagle, R.A.; Enriquez, M.; Grellet-Tinner, G.; Pérez-Huerta, A.; Hu, D.; Tütken, T.; Eiler, J.M. Isotopic ordering in eggshells reflects body temperatures and suggest differing thermophysiology in two Cretaceous dinosaurs. *Nat. Commun.* **2015**, *6*, 8296. [[CrossRef](#)] [[PubMed](#)]
67. Bischoff, W.D.; Sharma, S.K.; MacKenzie, F.T. Carbonate ion disorder in synthetic and biogenic magnesian calcites: A Raman spectral study. *Am. Mineral.* **1985**, *70*, 581–589.
68. Masic, A.; Weaver, J.C. Large area sub-micron chemical imaging of magnesium in sea urchin teeth. *J. Struct. Biol.* **2015**, *189*, 269–275. [[CrossRef](#)] [[PubMed](#)]
69. Thomas, D.B.; Hauber, M.E.; Hanley, D.; Waterhouse, F.I.N.; Fraser, S.; Gordon, K.C. Analysing avian eggshell pigments with Raman spectroscopy. *J. Exper. Biol.* **2015**, *218*, 2670–2674. [[CrossRef](#)]
70. Wedral, E.M.; Vadehra, D.V.; Baker, R.C. Chemical composition of the cuticle, and the inner and outer shell membranes from eggs of *Gallus gallus*. *Comp. Biochem. Physiol.* **1974**, *B47*, 361–640. [[CrossRef](#)]
71. Cusack, M.; Fraser, A.C.; Stachel, T. Magnesium and phosphorus distribution in the avian eggshell. *Comp. Biochem. Physiol.* **2003**, *B134*, 63–69. [[CrossRef](#)]
72. Hahn, E.N.; Sherman, V.R.; Pissarenko, A.; Rohrbach, S.D.; Fernandes, D.J.; Meyers, M.A. Nature’s technical ceramic: The avian eggshell. *J. R. Soc. Interface* **2017**, *14*, 20160804. [[CrossRef](#)]

Disclaimer/Publisher’s Note: The statements, opinions and data contained in all publications are solely those of the individual author(s) and contributor(s) and not of MDPI and/or the editor(s). MDPI and/or the editor(s) disclaim responsibility for any injury to people or property resulting from any ideas, methods, instructions or products referred to in the content.